



Efficacy of Smoothing Algorithms to Enhance Detection of Visual Field Progression in Glaucoma

Vahid Mohammadzadeh, MD,¹ Leyan Li, MS,^{2,3} Zhe Fei, PhD,^{2,3,4} Tyler Davis, MS,⁵ Esteban Morales, MS,¹ Kara Wu, BS,^{2,3} Elise Lee Ma, MD, PhD,¹ Abdelmonem Afifi, PhD,² Kouros Nouri-Mahdavi, MD, MS,¹ Joseph Caprioli, MD¹

Purpose: To evaluate and compare the effectiveness of nearest neighbor (NN)- and variational autoencoder (VAE)-smoothing algorithms to reduce variability and enhance the performance of glaucoma visual field (VF) progression models.

Design: Longitudinal cohort study.

Subjects: 7150 eyes (4232 patients), with ≥ 5 years of follow-up and ≥ 6 visits.

Methods: Visual field thresholds were smoothed with the NN and VAE algorithms. The mean total deviation (mTD) and VF index rates, pointwise linear regression (PLR), permutation of PLR (PoPLR), and the glaucoma rate index were applied to the unsmoothed and smoothed data.

Main Outcome Measures: The proportion of progressing eyes and the conversion to progression were compared between the smoothed and unsmoothed data. A simulation series of noiseless VFs with various patterns of glaucoma damage was used to evaluate the specificity of the smoothing models.

Results: The mean values of age and follow-up time were 62.8 (standard deviation: 12.6) years and 10.4 (standard deviation: 4.7) years, respectively. The proportion of progression was significantly higher for the NN and VAE smoothed data compared with the unsmoothed data. VF progression occurred significantly earlier with both smoothed data compared with unsmoothed data based on mTD rates, PLR, and PoPLR methods. The ability to detect the progressing eyes was similar for the unsmoothed and smoothed data in the simulation data.

Conclusions: Smoothing VF data with NN and VAE algorithms improves the signal-to-noise ratio for detection of change, results in earlier detection of VF progression, and could help monitor glaucoma progression more effectively in the clinical setting.

Financial Disclosure(s): Proprietary or commercial disclosure may be found in the Footnotes and Disclosures at the end of this article. *Ophthalmology Science* 2024;4:100423 © 2023 by the American Academy of Ophthalmology. This is an open access article under the CC BY-NC-ND license (<http://creativecommons.org/licenses/by-nc-nd/4.0/>).

Glaucoma is a progressive optic neuropathy and a leading cause of blindness worldwide.¹ It is characterized by progressive loss of retinal ganglion cells that causes visual functional loss and deterioration of the quality of life of glaucoma patients.^{2,3} Visual field (VF) testing is the standard modality for functional evaluation in glaucoma. Evaluation of longitudinal VF change is a fundamental approach for the detection of glaucoma progression; timely detection of disease deterioration would help preserve the functional abilities of glaucoma patients.⁴ Evaluation of rates of VF change is a practical method for detecting eyes with rapid progression of glaucoma.^{5–10} This important subset of glaucoma patients requires more aggressive management to slow the disease's course.

Several approaches have been used for identifying VF progression in glaucoma. The most common approach is clinical judgment. However, this approach is affected by high interobserver variability and well-known imprecision.^{11,12} Several statistical approaches have been

introduced for evaluating glaucoma progression. These methods consist of mean deviation rates of change, visual field index (VFI) rates of change, the Advanced Glaucoma Intervention Study and Collaborative Initial Glaucoma Treatment Study algorithms, pointwise linear regression (PLR), pointwise exponential regression (PER), permutation of pointwise linear regression (PoPLR), and glaucoma rate index (GRI).^{13–18} A study by Rabiolo et al has reported that PoPLR and GRI are the optimal methods for early detection of glaucoma progression.

Visual field testing is affected by short-term and long-term variability.^{19–23} There is strong evidence that the VF variability increases dramatically at locations with moderate loss of sensitivity.^{19–24} Visual field variability could result in false overdetection or underdetection of true glaucoma progression. Because only some of the factors influencing VF variability are known and most are not modifiable,^{24–28} designing methods that could address VF variability, without affecting the true signal (i.e., increasing

the signal-to-noise ratio), would enhance the detection of true glaucoma progression.

Several approaches have been used to address VF variability. Morales et al carried out various smoothing algorithms based on spatial clustering for reducing VF variability.²⁹ In that study, among the various smoothing algorithms,^{29–32} the nearest neighbor (NN) model performed best for improving forecasting of future VFs with regression models. In the NN model, the sensitivity at each location was weighted based on the sensitivity of adjacent locations and the distance between the adjacent locations. Another possible approach for reducing the variability of the VF test is to use deep learning (DL) models to project high-dimensional VF into low-dimensional latent features, which would be a summary of the original VF data.^{33–35} Subsequently, these low-dimensional latent space data can be mapped back to the reconstructed VF data. This is the basis of a DL generative model, known as a variational autoencoder (VAE).³⁶ The VAE and generative adversarial network are the 2 main generative DL models.^{36–38} Some studies have evaluated the performance of VAE for reducing the variability of longitudinal VF testing to improve the detection of glaucoma progression based on VF rates of change.^{39–41} It has been reported that the latent space of the VAE reveals novel physiologic patterns.^{42,43}

The purpose of this study was to investigate the utility of 2 different smoothing approaches (NN and VAE) for enhancing the detection of VF progression in a large data set of glaucomatous eyes with long follow-up.

Methods

Study Participants

Seven thousand one hundred fifty eyes (4232 patients) from the Glaucoma Division of Stein Eye Institute, University of California, Los Angeles, were included in this retrospective longitudinal study. University of California, Los Angeles' Institutional Review Board approved this study and the study adhered to the tenets of the Declaration of Helsinki and the Health Insurance Portability and Accountability Act policies. Eligible eyes were required to have ≥ 6 VF examinations available and a minimum follow-up of 3 years.

VF. Standard automated perimetry was carried out with Humphrey Field Analyzer II (Carl Zeiss Meditec). The reliability criteria were a false positive rate $\leq 15\%$ and fixation loss and false negative rates $\leq 30\%$. The threshold sensitivities and total deviation (TD) values of the 54 locations belonging to 24-2 VF and the VFI were exported as XML files. The values for locations 26 and 35 were omitted since for most of the eyes, those locations correspond to the blind spot. In this study, instead of evaluating the exported mean deviation from the device, we used the *visualFields* package from R programming to convert the threshold sensitivities to TDs and, subsequently, averaged the TDs of the 52 locations into a single value called mean total deviation (mTD).⁴⁴

Study Design

Data smoothing approaches. *NN smoothing approach.* The NN approach has been previously described by Morales et al.²⁹ The threshold sensitivities at each VF location were reconstructed based on its distance from adjacent neighboring locations and the

threshold of the adjacent neighboring locations. The minimum number of possible neighbors was 4, and the maximum number of possible neighbors was 8. The following equation was used for smoothing threshold sensitivities based on the distance and sensitivities of neighboring locations:

$$VF_{new} = \frac{1}{2} \times VF_{raw} + \frac{1}{2} \frac{\sum_1^n (w \times VF_{Neighbor})}{\sum_1^n (w)}$$

where distance (d) = 1 (for adjacent VF locations), weight (w) = $1/d^2$, n = number of neighboring VF locations, Vo_{cation} = decibels (dB) value of VF location being weighted, VF_{New} is the output smoothed dB value, VF_{raw} is the input raw dB value, and $VF_{Neighbor}$ = dB value of neighboring VF locations. The mTD and VFI were estimated after smoothing the threshold sensitivities with the *visualFields* R package, as explained above.⁴⁴

VAE. We used a VAE to reconstruct all the VF test images.³⁶ The model consisted of an encoder with 2 hidden layers, a decoder with 2 hidden layers, and an 8-dimensional latent space where the inputs were encoded as 8 probability distributions. The hidden layers had 38 and 26 units, respectively. These layer sizes were selected following the work of Asaoka et al.⁴⁰ The final layer used a sigmoid activation function to generate a vector with a range (0, 1) of the same length as the input. Figure 1 illustrates the structure of the VAE. The model was trained to minimize the weighted sum of mean squared error as a reconstruction loss and the Kullback–Leibler divergence between the encoded distributions and a Gaussian distribution as regularization.⁴⁵ We weighted the sum by multiplying the reconstruction loss by a weight factor. We explored 3 weight factors and selected the one with the best validation mean squared error. The explored values comprise a Kullback–Leibler divergence heavy sum, with reconstruction weight 1, a balanced sum, with reconstruction weight equal to the number of batches in the training set, and a reconstruction loss heavy sum, with weight equal to 10 000 times the length of an input vector divided by the batch size. The encoder input is minimum to maximum scaled between 0 and 1, and the decoder output is transformed back to the original scale. The model is trained with a batch size of 32 for 500 epochs. Loss is optimized with the Adam optimizer with a learning rate of 0.001.⁴⁶ We used a data set of 173 101 VF visits from 66 123 eyes and an 80%/10%/10% train/validation/test split. If an eye appeared multiple times in our data set, its VFs were contained entirely within a single data set split. For the further analysis of this study, we selected 7150 eyes (minimum of 3 years of follow-up and 6 visit dates) from the training and validation data set of these VAE data. The VAE is implemented in TensorFlow 2.6.0⁴⁷ and Python 3.9.13.⁴⁸ Scikit-learn 1.0.2⁴⁹ is used for generating the data split and Scipy 1.8.0⁵⁰ is used for calculating statistics. Code for training and evaluating the VAE is publicly available on GitHub.

VF Progression Methods. Two global VF progression methods (mTD and VFI rates) and 3 localized VF progression methods (PLR, PoPLR, and GRI) were applied to the unsmoothed data, and the NN smoothed and the VAE smoothed data. For each method, we performed the analyses starting with 6 visits and repeated them sequentially by adding 1 visit at a time until the last follow-up. The criteria for the definition of glaucoma progression are explained below for each approach; an eye was labeled as progressing if the criteria were met at 2 consecutive points and at the last follow-up visit (i.e., including the entire data set of an eye).

mTD and VFI Rates. Linear regression of mTD and VFI measurements against time was performed. Progression was

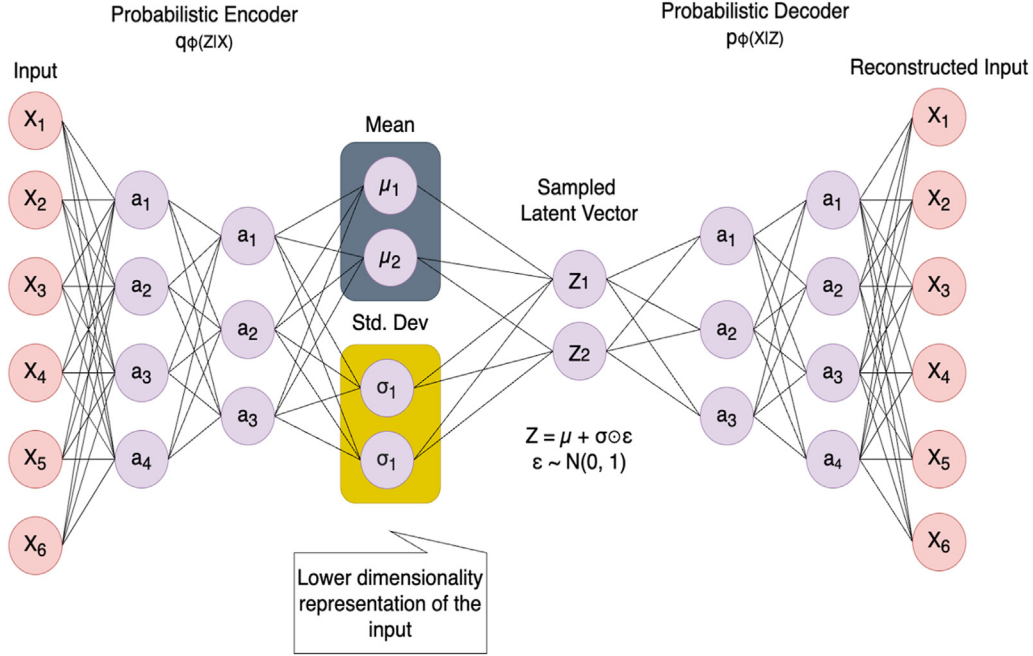


Figure 1. The structure of the variational autoencoder used in this study. The model consisted of an encoder with 2 hidden layers, a decoder with 2 hidden layers, and an 8-dimensional latent space in which the inputs were encoded as 8 probability distributions. The autoencoder first uses 2 hidden layers (a_x , left hand side) to generate a lower dimensionality probabilistic representation of the input. This representation consists of a set of Gaussian distributions, each with a particular mean (μ) and standard deviation (σ). To reconstruct the input, each distribution is sampled by adding a random value (ϵ) times the standard deviation to the mean. Two hidden layers (a_x , right hand side) then decode this sampled representation to reconstruct the input as accurately as possible.

defined as mTD rates ≤ -0.5 dB per year and VFI rates $\leq -1\%$ per year along with a P value ≤ 0.05 .¹⁷

PLR. The slope of the regression line of the threshold sensitivity against time for each of the 52 VF locations, expressed in decibels per year, was defined as the pointwise linear rate of change. Progression was defined as presence of 3 pointwise series having a significant regression slope ($P \leq 0.01$) and rates of change of ≤ -1 dB per year. Pointwise linear regression analysis regresses sensitivity values of each location on its follow-up variable by SLR. The progression of the VF is derived from the number of significant decaying locations in the VF.

PoPLR. This method has been previously described by O’Leary et al.¹⁶ The pointwise linear regression of TD values against time was performed in each eye and the slope from each location in the VF was combined to calculate S statistics (S_{obs}). The P values for every location were also combined using the following equation (Fisher method)⁵¹:

$$S = - \sum_{i=1}^n \ln(p_i) k_i$$

where k_i is 1 if $P_i < 0.05$ or else 0. The smallest P value is used if none of the locations has $P_i < 0.05$.

In the next step, the patient’s original VF sequence was then randomly reordered up to 5000 times, and a global score, called S_p , was obtained from each permutated series. Finally, S_{obs} was compared with the distribution of S_p , and the statistical significance was derived from the ranking of S_{obs} within the S_p distribution. A P value < 0.05 was labeled as progression.

GRI. This method was previously described by Caprioli et al.¹⁸ Glaucoma rate index analysis assigns a score ranging from 0 to 100 to each eye, which represents the rate of deterioration from

very fast decay (100) to stable (GRI = 0); improving eyes demonstrate a negative GRI. The pointwise rate of change (PRC) is calculated after fitting a PER and removing outliers (determined by a Cook distance > 1 and studentized residual > 3), adjusting for age and location. A decay PER model is expressed as $S = e^{(a+b*FU)}$, where b is the slope. An improved PER model is expressed as $S_0 - S = e^{(a+b*FU)}$, where S_0 is the normal threshold value at a given age plus 2 SD and b is the slope. The pointwise rate of change is calculated as the proportion of change per year of the entire perimetric range correcting for location and age. The GRI score is calculated by summing the PRC of all detected progressive locations, normalized from -100 to $+100$.

Simulation Setting. To determine whether the 2 smoothing approaches would potentially address the noise without negatively affecting the true signal, we designed several noise-free simulation VF data demonstrating different patterns of focal glaucoma progression and diffuse progression patterns, including age effect and cataract-induced sensitivity decrease. We performed the simulation algorithm previously published by our team.¹⁷

The R platform (R Foundation for Statistical Computing) was used to design the algorithm based on the models described previously.^{52,53} The following steps were performed for this purpose:

1. The software defines the baseline threshold sensitivities, follow-up length, pointwise rates of progression annually, and the number of VF examinations. Tests are equally spaced over the follow-up period, and the ratio between the number of VFs and the length of the simulation was considered for defining the frequency of visits.
2. Linear regression was applied for every test location. An additional decay of 0.1 dB per year is added to simulate

age-related decline, which was independent of the rate of progression.⁵⁴

- The difference between the simulation data evaluated in this study compared with the study by Rabiolo et al¹⁷ was that only noise-free simulation data was considered for the purpose of investigating the efficacy of the smoothing approach not affecting the true signal.

The *visualFields* R package is able to generate the VFI, TD values, and the TD probability map for simulated data.⁴⁴

Twenty-five simulations with a total of 67 eyes were generated. The simulation length was set at 9.5 years. Biannual testing frequency for a total of 20 VFs was defined. The baseline age was set at 60 years. Two VF examinations from actual glaucoma patients, one with a focal inferior nasal defect and another with a superior arcuate scotoma, were chosen as the 2 baselines. In the next step, 2 patterns of focal decay and diffuse decay were calculated as follows:

- Focal decay, in which 4 (small scotoma), 8 (medium scotoma), or 16 (large scotoma) locations significantly deteriorate. Small defects were a nasal scotoma and a paracentral scotoma. Medium-sized defects consisted of a nasal step and an arcuate scotoma extending to 5 degrees from fixation. Large defects comprised of 2 broad inferior and superior arcuate scotomas. Three different rates of progression, -0.5 , -1.0 , and -2.0 dB per year, were applied to deteriorating locations in addition to normal age-related decay.
- Diffuse decay was defined as every location undergoing the same rate of progression.

Based on the baseline examinations, rates, and patterns of progression, 24 scenarios were simulated: eyes with focal decay, demonstrating deterioration of simulated scotomas, and eyes with diffuse decay were considered as progressing; eyes with simulated age-related and cataract-related decay were considered as nonprogressing.

Study End Points and Statistical Analysis

The proportion of the eyes defined as progressing was calculated for each VF progression method for the unsmoothed, NN-smoothed, and VAE-smoothed data. The time-to-detect progression (TDP) for each VF progression method was defined as the first follow-up time where the criteria of VF progression were met with confirmation on a subsequent visit.

To better evaluate the time to VF progression, we performed survival analyses. Analogous to an interval-censored survival outcome, the conversion time for each progressive eye is determined by sequentially conducting the progression analysis with data truncated at different visits, which imitates a clinical setting where each metric is calculated at every visit. The minimum number of visits is set at 6 to ensure the model's reliability. Like the previous approach, we carried out each method of progression detection, starting from the 6th visit and subsequently adding 1 visit and repeating the analysis. Then, the conversion time was determined by the first visit time when progression was established. For example, for an eye with a total of 8 visits, 3 sets of regression analyses will be fitted starting with the 6th through the 8th visit in the series. If the progression conclusion sequence is (0, 1, 1), with 1 indicating progression then the conversion of this eye occurs at its 7th visit, and conversion time is the follow-up time from the 1st visit to the 7th visit.

The mean conversion time of reconstructed data was reported in all 5 methods for the unsmoothed, NN-smoothed and VAE-smoothed data. A total of 3 pairwise *P* values were calculated for

each VF progression method. To be conservative, we applied Bonferroni adjustment, with *P* values $\leq 0.05/3 = 0.0167$ as statistically significant. Furthermore, the conversion time was considered as a survival variable, to gain more power and prevent potential information loss on testing directly on the mean. That is, eyes that were nonprogressive were censored at their last visit. Kaplan–Meier curves were plotted, and pairwise log-rank tests were applied to assess the differences.

To ensure that smoothing approaches do not introduce an untoward influence on the true glaucoma signal, first, the NN and VAE smoothing approaches were applied to the simulation data. Then the 5 VF progression models were applied to the unsmoothed, NN-smoothed, and VAE-smoothed simulation data. The ground truth was the number of progressing eyes based on focal decay and diffuse decay. The number of eyes defined as progressing based on each of the VF-progression models on the unsmoothed, NN-smoothed, and VAE-smoothed data were compared with the ground truth. For representing this analysis, we plotted a Cleveland Dot Plot, which showed the agreement of the unsmoothed, NN-smoothed, and VAE-smoothed data for identifying progression based on each of the VF-progression methods.

Results

Seven thousand one hundred fifty eyes (from 4232 patients) were included in this study. Four thousand one hundred sixty-three examinations from 2201 eyes were excluded, based on the VF exclusion criteria, and a total of 71 542 VF examinations (from 7150 eyes) were included in the study. The mean values of baseline age and follow-up time were 62.8 (standard deviation: 12.6) years and 10.4 (standard deviation: 4.7) years. The mean values of baseline and final logMAR visual acuity were 0.15 (standard deviation: 0.26) and 0.16 (standard deviation: 0.28), respectively. The demographic characteristics of the study eyes are presented in Table 1.

The proportion of the eyes demonstrating VF progression based on the 5 methods for the unsmoothed, NN-smoothed,

Table 1. Demographic Characteristics of the Study Eyes

	N = 4232 (Eyes = 7155)
Age, mean (SD), yrs	62.8 (12.67)
Sex	
Female	2262 (53%)
Male	1970 (47%)
Race	
White	2506 (59%)
African American	317 (7%)
Asian	542 (13%)
Hispanic	43 (1%)
Others	824 (20%)
Visual field frequency, median (IQR)	9 (7–12)
Baseline visual field mean deviation, average (SD), dB	−3.94 (5.11)
Final visual field mean deviation, average (SD), dB	−5.63 (6.32)
Follow-up time, mean (SD), yrs	10.4 (4.72)
Baseline visual acuity (SD), logMAR	0.15 (0.26)
Final visual acuity (SD), logMAR	0.16 (0.28)

dB = decibels; IQR = interquartile range; logMAR = logarithm of the minimum angle of resolution; SD = standard deviation.

Table 2. The Proportion of Progressing Eyes for 5 Visual Field Progression Methods for the Unsmoothed, the NN Smoothed, and Variational Autoencoder Smoothed Data

VF Progression Method	Unsmoothed Data	VAE Smoothed	NN Smoothed	Unsmoothed vs. NN Smoothed	Unsmoothed vs. VAE Smoothed	NN vs. VAE
mTD rates	874 (12.2%)	974 (13.6%)	1010 (14.1%)	< 0.001	< 0.001	0.048
VFI rates	1002 (14%)	962 (13.4%)	1002 (14.0%)	NA	0.045	0.045
PLR	1029 (14.3%)	1152 (16.1%)	1137 (15.8%)	< 0.001	< 0.001	0.463
GRI	1917 (26.7%)	2033 (28.4%)	2077 (29.0%)	< 0.001	< 0.001	0.064
PoPLR	2977 (41.6%)	3310 (46.2)	3618 (50.5%)	< 0.001	< 0.001	< 0.001

The database consisted of 7155 eyes of 4232 patients.

GRI = glaucoma rate index; mTD = mean of total deviation; NA = not available; NN = nearest neighbor; PLR = pointwise linear regression; PoPLR = permutation of pointwise linear regression; VAE = variational autoencoder; VF = visual field; VFI = visual field index.

and VAE-smoothed data are given in Table 2. The proportion of progressing eyes was significantly higher for NN-smoothed and VAE-smoothed data than that of the unsmoothed data for the mTD rates, PLR, GRI, and PoPLR. The comparison of the proportion of progressing eye between the 5 methods for VF progression for each data set revealed that the proportion was highest in GRI, followed by PoPLR, PLR, mTD rates, and then VFI rates. The TDP was significantly earlier for the NN-smoothed and VAE-smoothed data compared unsmoothed data for PLR (7.3, 7.6, and 8.2 years, respectively; P value < 0.001) and PoPLR (6.8, 7.1 and 7.6 years, respectively; P value < 0.001). Table 3 shows the results of the TDP analyses.

The results of the conversion survival analysis strongly support the previous findings. This analysis demonstrated that the NN smoothed and VAE smoothed data had lower survival probabilities over time for most of the VF progression methods, which means the smoothing approaches were able to provide earlier detection of glaucoma progression. A pairwise log-rank test with Bonferroni adjustment was applied to the pairwise comparisons among the 3 data sets (Table 4). The VAE smoothed data outperforms the unsmoothed data with mTD rates, PLR, and POPLR progression methods. The NN-smoothed data outperforms unsmoothed data within all VF progression methods, except for that of VFI rates. For comparison between VAE-smoothed and NN-smoothed data, the NN-smoothed data demonstrated better performance than VAE-smoothed data in mTD rates and POPLR analysis. Figure 2 represents the Kaplan–Meier curves of the survival analysis for each of the VF progression methods. For the mTD rates, PLR, and PoPLR, both the NN-smoothed and VAE-smoothed data had lower survival probabilities compared with the unsmoothed data. For GRI, only NN-smoothed data had a lower survival probability compared with the unsmoothed data.

We also investigated whether the smoothing algorithms preserved the true glaucoma signal. We found that for most of the simulation data, the number of progressing eyes from each of the 5 VF progression models was similar for the unsmoothed, NN-smoothed, and VAE-smoothed simulation data regarding the actual number of progressing

eyes in the noise-free simulation data (ground truth). For the simulations with focal decay (rates = -0.5 dB per year), in the VF progression methods, the VAE- and NN-smoothed data demonstrated the number of progressing eyes were closer to the ground truth compared with the unsmoothed data.

Discussion

In this study, we evaluated the performance of NN- and VAE-smoothing approaches for improving the detection of VF progression in eyes with glaucoma. The proportion of eyes defined as progressing according to mTD rates, VFI rates, PLR, PoPLR, and GRI was calculated for the unsmoothed, NN-smoothed and VAE-smoothed data and compared between them. We also evaluated the TDP with survival analysis. For mTD rates, PLR, PoPLR, and GRI, the proportion of progressing eyes was higher for the smoothed data compared with unsmoothed data. The TDP occurred significantly earlier for the NN- and VAE-smoothed data compared with unsmoothed data for the PLR and PoPLR progression methods. Based on survival analyses, the NN-smoothed data detected VF progression earlier compared with the unsmoothed data for all the VF-progression methods, except VFI rates. The VAE-smoothed data led to earlier detection of glaucoma progression compared with unsmoothed data for the mTD rates, PLR, and PoPLR methods. The results from the noise-free simulation data showed that the smoothing approaches did not introduce a negative effect on the VF true signal while reducing variability. Therefore, this study provides evidence that applying smoothing methods to VF data enhances detection of glaucoma progression resulting in earlier identification of change.

The VAE is a DL model that consists of an encoder compressing the data into a latent space through sampling and principal component analysis together with a unique decoder that is able to regenerate the data.³⁶ Therefore, it is able to provide more realistic data compared with models only equipped with the compression process, such as factor analysis and independent component analysis.^{55,56} Another advantage of the VAE compared with other

Table 3. The TDP for the 5 Visual Field Progression Methods Investigated in This Study and Comparison of TDP between Unsmoothed, NN Smoothed, and VAE Smoothed Data

VF Progression Method	Unsmoothed Data TTP	VAE Smoothed Data TTP	NN Smoothed TTP	Unsmoothed vs. VAE Smoothed P Value	Unsmoothed vs. NN Smoothed P Value	NN Smoothed and VAE Smoothed P Value
mTD rates	8.28	8.58	8.43	0.009	0.179	0.181
VFI rates	8.21	8.23	8.21	0.940	0.870	0.810
GRI	7.24	7.46	7.38	0.037	0.098	0.654
PLR	8.20	7.64	7.36	< 0.001	< 0.001	0.276
PoPLR	7.68	7.17	6.86	< 0.001	< 0.001	0.103

GRI = glaucoma rate index; mTD = mean of total deviation; NN = nearest neighbor; PLR = pointwise linear regression; PoPLR = permutation of pointwise linear regression; TDP = time to detect progression; VAE = variational autoencoder; VF = visual field; VFI = visual field index. Boldface indicates statistical significance.

methods is that, because VAE is a DL model, it can handle nonlinear patterns in the data set.

One advantage of the VAE over other DL models for investigating VF progression is that VAE considers the original VF data as the ground truth for training, although other DL models use other approaches as the ground truth, such as clinical decision statistical methods based on the VF data, which could introduce significant noise into the training model because of a lack of a gold standard for defining the classification.^{57–59} In our study, after applying the VAE on the original VF data, the ability to detect glaucoma progression was enhanced by detecting higher proportions of progressing eyes through the VF progression methods and resulted in significantly earlier detection of glaucoma progression with mTD rates, PLR, and PoPLR progression methods. These findings, along with the physiologic feasibility of the latent space of the VAE model, suggest it is an interesting approach for improving the clinical task of monitoring glaucoma progression.^{42,43}

The NN-smoothing algorithm also improved the ability to detect glaucoma progression with various VF-progression models. The proportion of the eyes demonstrating glaucoma progression was higher compared with the original unsmoothed data. Additionally, after performing NN smoothing, glaucoma progression was detected significantly earlier compared with when unsmoothed data were used for all the VF-progression models except VFI rates. The NN-smoothing algorithm was initially introduced by Morales et al.²⁹

The biggest advantage of this algorithm, compared with the more complicated VAE model, is that simple calculations are required. The NN- and VAE-smoothing models demonstrated a similar performance for the detection of glaucoma progression except that the analyses using NN-smoothed data led to earlier detection of glaucoma progression with the mTD rates and PoPLR. The NN algorithm decreases the variability by averaging the threshold sensitivities in a localized manner, resulting in a less noisy VF data.⁶⁰

Five trend-based analyses for defining glaucoma progression were evaluated in this study. Trend-based analysis has several advantages over event-based analysis including better predictability.⁶¹ More specifically, pointwise trend-based analyses have benefits over global values (mean deviation and VFI) trend-based analysis, such as the ability to detect early localized glaucomatous defects and monitor the pattern of the VF progression by preserving spatial information.⁶² There is no universally recognized best approach for detecting glaucoma progression based on VF. Rabiolo et al reported that GRI and PoPLR both identified a higher proportion of progression and detected disease deterioration earlier compared with event-based and other trend-based methods tested.¹⁷ We also found that GRI and PoPLR found a higher proportion of progressing eyes, compared with other VF progression methods for both the unsmoothed and smoothed data. It should be noted that the methodology for performing the GRI already

Table 4. The Pairwise Log-Rank Test for Comparing the Time to Conversion to Glaucoma Progression Based on Survival Analysis for the 5 Methods Investigated in This Study

VF progression method	Pairwise Log-Rank Test P Values		
	Unsmoothed vs. VAE Smoothed	Unsmoothed vs. NN Smoothed	VAE Smoothed vs. NN Smoothed
mTD	< 0.001	< 0.001	< 0.001
VFI	0.331	0.740	0.521
GRI	0.045	0.005	0.433
PLR	0.0037	0.01	0.746
PoPLR	< 0.001	< 0.001	< 0.001

GRI = glaucoma rate index; mTD = mean of total deviation; NN = nearest neighbor; PLR = pointwise linear regression; PoPLR = permutation of pointwise linear regression; VAE = variational autoencoder; VF = visual field; VFI = visual field index. Boldface indicates statistical significance.

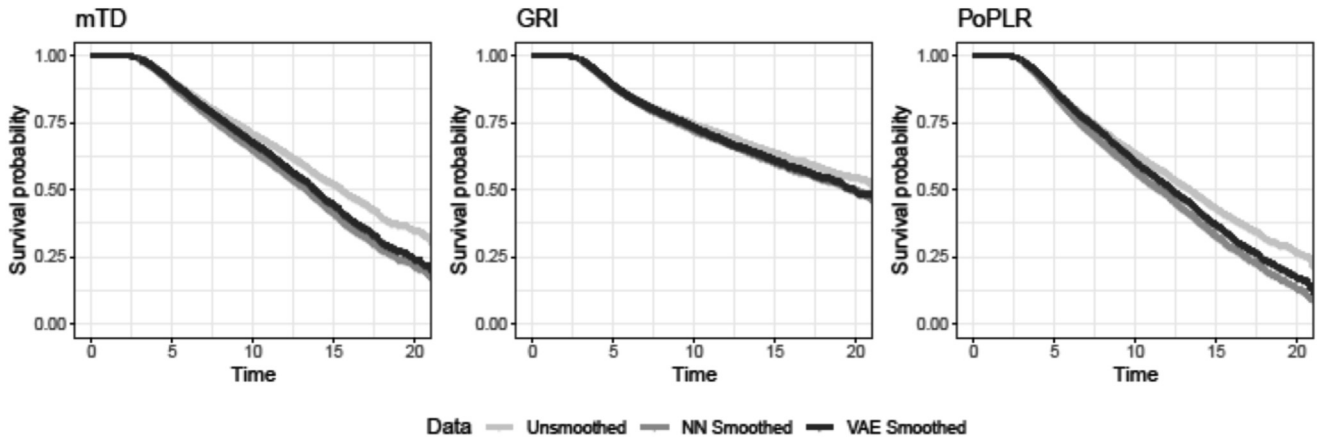


Figure 2. The Kaplan–Meier curves for time to detect progression with 3 of the explored approaches, the mean total deviation (mTD) rates, glaucoma rate index (GRI), and permutation of pointwise linear regression (PoPLR).

incorporates some smoothing of the VF data.¹⁸ Additionally, PLR and PoPLR used the NN- and VAE-smoothed data compared with unsmoothed, whereas GRI had this advantage only with the NN-smoothed data. We included a larger number of eyes compared with the study by Rabiolo et al and found a similar finding about GRI and PoPLR, which supports the utility of these methods for evaluating glaucoma progression.

When applying an algorithm to reduce variability, it is important to have confirmation that the algorithm does not have a negative effect on the true glaucoma “signal.” For this purpose, we generated 24 noise-free VF progression simulations, which included eyes with different patterns of focal and global changes over time (ground truth). We applied the 5 VF progression methods on these noise-free simulations before and after applying the smoothing algorithms (NN and VAE). For most of the simulations, the number of the progressing eyes was similar for the unsmoothed, the NN-smoothed and the VAE-smoothed data with the ground truth. The number of progressing eyes defined by PLR, PoPLR, and GRI was different from the ground truth for the unsmoothed data, and the NN- and VAE-smoothed data in the simulation VF series showing a small focal defect; this could be explained by limitations of the pointwise trend-based models for detecting small glaucoma defects and not the effect of the smoothing algorithms on the true glaucoma signal. In addition, for some of the focal glaucoma progression simulations, the number of deteriorating eyes defined by PLR, PoPLR, and GRI were closer to the ground truth for the NN- and VAE-smoothed data, compared with the unsmoothed data. These findings confirm that applying smoothing algorithms efficiently

reduces variability while preserving the true glaucoma signal; this could explain how applying these algorithms to the original VF data resulted in the detection of glaucoma progression earlier and more frequently.

There are some limitations to our study. For the simulations, we did not introduce Gaussian distributions and variability as we have done in our previous work.¹⁷ The variability introduced by the Gaussian distribution and standard deviation would have introduced distinct patterns of variability that would not be efficiently learned by the VAE model. Therefore, they could not be used for the purpose of investigating the efficacy of VAE for preserving the true glaucoma signal. Future implementations of VAE model structures could solve this issue. The frequency of VF testing was not similar across the eyes in the study, which could have affected the TDP.⁶³ Another limitation of our study is that there was a slight difference in visual acuity between the baseline and final visits. This could be explained by the fact that glaucoma mainly involves the peripheral VF, and the central visual acuity is involved in the final stages of the disease. However, the main outcome of this study was to investigate various methods of glaucoma progression based on VF.

In conclusion, reducing the variability and smoothing VF data with NN and VAE models resulted in the detection of a higher proportion of progressing eyes and earlier detection of glaucoma progression with various VF progression methods, while maintaining the specificity of the VF data. Among the VF progression methods, the pointwise trend-based methods, especially GRI and PoPLR, demonstrated the highest performance in the detection of glaucoma progression with the smoothed VF data.

Footnotes and Disclosures

Originally received: May 10, 2023.

Final revision: September 27, 2023.

Accepted: October 31, 2023.

Available online: November 4, 2023. Manuscript no. XOPS-D-23-00098R1.

¹ David Geffen School of Medicine, Glaucoma Division, Jules Stein Eye Institute, Los Angeles, California.

² University of California Los Angeles Jonathan and Karin Fielding School of Public Health, Los Angeles, California.

³ Biostatistics, University of California Los Angeles, Los Angeles, California.

⁴ Department of Statistics, University of California, Riverside, California.

⁵ Computer Science, University of California Los Angeles, Los Angeles, California.

Disclosure(s):

All authors have completed and submitted the ICMJE disclosures form.

The authors have no proprietary or commercial interest in any materials discussed in this article.

The author(s) have made the following disclosures:

K.N.M.: Financial support - Unrestricted departmental grant from Research to Prevent Blindness, NIH grant R01-EY029792 Payden Glaucoma Fund, Simms/Mann Family Foundation, and an unrestricted research grant from Heidelberg Engineering

The sponsor or funding organization had no role in the design or conduct of this research.

HUMAN SUBJECTS: Human subjects were included in this study. University of California, Los Angeles' Institutional Review Board approved this study and the study adhered to the tenets of the Declaration of Helsinki and the Health Insurance Portability and Accountability Act policies. The requirement for informed consent was waived because of the retrospective nature of the study.

No animal subjects were used in this study.

Author Contributions:

Conception and design: Mohammadzadeh, Li, Fei, Davis, Morales, Wu, Ma, Afifi, Nouri-Mahdavi, Caprioli

Data collection: Mohammadzadeh, Li, Fei, Davis, Morales, Wu, Ma, Afifi, Nouri-Mahdavi, Caprioli

Analysis and interpretation: Mohammadzadeh, Li, Fei, Davis, Morales, Wu, Ma, Afifi, Nouri-Mahdavi, Caprioli

Obtained funding: Caprioli, Nouri-Mahdavi

Overall responsibility: Mohammadzadeh, Li, Fei, Davis, Morales, Wu, Ma, Afifi, Nouri-Mahdavi, Caprioli

Abbreviations and Acronyms:

DL = deep learning; **GRI** = glaucoma rate index; **mTD** = mean of total deviation; **NN** = nearest neighbor; **PER** = pointwise exponential regression; **PLR** = pointwise linear regression; **PoPLR** = permutation of pointwise linear regression; **TD** = total deviation; **TDP** = time to detect progression; **VAE** = variational autoencoder; **VF** = visual field; **VFI** = visual field index.

Keywords:

Artificial intelligence, Glaucoma progression, Variability, Variational autoencoder, Visual field, Visual field noise.

Correspondence:

Joseph Caprioli, MD, 100 Stein Plaza, Los Angeles, CA, 90095. E-mail: caprioli@jsei.ucla.edu.

References

- Quigley HA, Broman AT. The number of people with glaucoma worldwide in 2010 and 2020. *Br J Ophthalmol*. 2006;90:262–267. <https://doi.org/10.1136/bjo.2005.081224>.
- Otarola F, Chen A, Morales E, Yu F, Afifi A, Caprioli J. Course of glaucomatous visual field loss across the entire perimetric range. *JAMA Ophthalmol*. 2016;134:496–502. <https://doi.org/10.1001/jamaophthalmol.2016.0118>.
- Quaranta L, Riva I, Gerardi C, Oddone F, Floriani I, Konstas AG. Quality of life in glaucoma: a review of the literature. *Adv Ther*. 2016;33:959–981. <https://doi.org/10.1007/s12325-016-0333-6>.
- Caprioli J. The importance of rates in glaucoma. *Am J Ophthalmol*. 2008;145:191–192. <https://doi.org/10.1016/j.ajo.2007.12.003>.
- Caprioli J, Mock D, Bitrian E, et al. A method to measure and predict rates of regional visual field decay in glaucoma. *Invest Ophthalmol Vis Sci*. 2011;52:4765–4773. <https://doi.org/10.1167/iovs.10-6414>.
- Johnson CA, Cioffi GA, Drance SM, et al. A multicenter comparison study of the Humphrey Field Analyzer I and the Humphrey Field Analyzer II. *Ophthalmology*. 1997;104:1910–1917. [https://doi.org/10.1016/s0161-6420\(97\)30008-6](https://doi.org/10.1016/s0161-6420(97)30008-6).
- Reis AS, Artes PH, Belliveau AC, et al. Rates of change in the visual field and optic disc in patients with distinct patterns of glaucomatous optic disc damage. *Ophthalmology*. 2012;119:294–303. <https://doi.org/10.1016/j.ophtha.2011.07.040>.
- Advanced glaucoma intervention study. 2. Visual field test scoring and reliability. *Ophthalmology*. 1994;101:1445–1455. [https://doi.org/10.1016/S0161-6420\(94\)31171-7](https://doi.org/10.1016/S0161-6420(94)31171-7).
- Heijl A, Leske MC, Bengtsson B, Bengtsson B, Hussein M; Early Manifest Glaucoma Trial Group. Measuring visual field progression in the Early Manifest Glaucoma Trial. *Acta Ophthalmol Scand*. 2003;81:286–293. <https://doi.org/10.1034/j.1600-0420.2003.00070.x>.
- Schulzer M, Airaksinen PJ, Alward WLM. Intraocular pressure reduction in normal-tension glaucoma patients. The Normal Tension Glaucoma Study Group. *Ophthalmology*. 1992;99:1468–1470. [https://doi.org/10.1016/s0161-6420\(92\)31782-8](https://doi.org/10.1016/s0161-6420(92)31782-8).
- Aref AA, Budenz DL. Detecting visual field progression. *Ophthalmology*. 2017;124:S51–S56. <https://doi.org/10.1016/j.ophtha.2017.05.010>.
- Tanna AP, Bandi JR, Budenz DL, et al. Interobserver agreement and intraobserver reproducibility of the subjective determination of glaucomatous visual field progression. *Ophthalmology*. 2011;118:60–65. <https://doi.org/10.1016/j.ophtha.2010.04.038>.
- Gardiner SK, Demirel S. Detecting change using Standard global perimetric indices in glaucoma. *Am J Ophthalmol*. 2017;176:148–156. <https://doi.org/10.1016/j.ajo.2017.01.013>.
- Chen A, Nouri-Mahdavi K, Otarola FJ, Yu F, Afifi AA, Caprioli J. Models of glaucomatous visual field loss. *Invest Ophthalmol Vis Sci*. 2014;55:7881–7887. <https://doi.org/10.1167/iovs.14-15435>.
- Viswanathan AC, Fitzke FW, Hitchings RA. Early detection of visual field progression in glaucoma: a comparison of progressor and StatPac 2. *Br J Ophthalmol*. 1997;81:1037–1042. <https://doi.org/10.1136/bjo.81.12.1037>.
- O'Leary N, Chauhan BC, Artes PH. Visual field progression in glaucoma: estimating the overall significance of deterioration with permutation analyses of pointwise linear regression (PoPLR). *Invest Ophthalmol Vis Sci*. 2012;53:6776–6784. <https://doi.org/10.1167/iovs.12-10049>.
- Rabiolo A, Morales E, Mohamed L, et al. Comparison of methods to detect and measure glaucomatous visual field progression. *Transl Vis Sci Technol*. 2019;8:2. <https://doi.org/10.1167/tvst.8.5.2>.
- Caprioli J, Mohamed L, Morales E, et al. A method to measure the rate of glaucomatous visual field change, 14–14 *Transl Vis Sci Technol*. 2018;7. <https://doi.org/10.1167/tvst.7.6.14>.

19. Artes PH, Iwase A, Ohno Y, Kitazawa Y, Chauhan BC. Properties of perimetric threshold estimates from Full threshold, SITA Standard, and SITA Fast strategies. *Invest Ophthalmol Vis Sci.* 2002;43:2654–2659.
20. Russell RA, Crabb DP, Malik R, Garway-Heath DF. The relationship between variability and sensitivity in large-scale longitudinal visual field data. *Invest Ophthalmol Vis Sci.* 2012;53:5985–5990. <https://doi.org/10.1167/iovs.12-10428>.
21. Gardiner SK. Differences in the relation between perimetric sensitivity and variability between locations across the visual field. *Invest Ophthalmol Vis Sci.* 2018;59:3667–3674. <https://doi.org/10.1167/iovs.18-24303>.
22. Heijl A, Lindgren A, Lindgren G. Test-retest variability in glaucomatous visual fields. *Am J Ophthalmol.* 1989;108:130–135. [https://doi.org/10.1016/0002-9394\(89\)90006-8](https://doi.org/10.1016/0002-9394(89)90006-8).
23. Henson DB, Chaudry S, Artes PH, Faragher EB, Ansons A. Response variability in the visual field: comparison of optic neuritis, glaucoma, ocular hypertension, and normal eyes. *Invest Ophthalmol Vis Sci.* 2000;41:417–421.
24. Rabiolo A, Morales E, Kim JH, et al. Predictors of long-term visual field fluctuation in glaucoma patients. *Ophthalmology.* 2020;127:739–747. <https://doi.org/10.1016/j.ophtha.2019.11.021>.
25. Artes PH, O’Leary N, Hutchison DM, et al. Properties of the StatPac visual field index. *Invest Ophthalmol Vis Sci.* 2011;52:4030–4038. <https://doi.org/10.1167/iovs.10-6905>.
26. Wall M, Doyle CK, Eden T, Zamba KD, Johnson CA. Size threshold perimetry performs as well as conventional automated perimetry with stimulus sizes III, V, and VI for glaucomatous loss. *Invest Ophthalmol Vis Sci.* 2013;54:3975–3983. <https://doi.org/10.1167/iovs.12-11300>.
27. Yohannan J, Wang J, Brown J, et al. Evidence-based criteria for assessment of visual field reliability. *Ophthalmology.* 2017;124:1612–1620. <https://doi.org/10.1016/j.ophtha.2017.04.035>.
28. Gracitelli CPB, Zangwill LM, Diniz-Filho A, et al. Detection of glaucoma progression in individuals of African descent compared with those of European descent. *JAMA Ophthalmol.* 2018;136:329–335. <https://doi.org/10.1001/jamaophthalmol.2017.6836>.
29. Morales E, de Leon JM, Abdollahi N, Yu F, Nouri-Mahdavi K, Caprioli J. Enhancement of visual field predictions with pointwise exponential regression (PER) and pointwise linear regression (PLR). *Transl Vis Sci Technol.* 2016;5:12. <https://doi.org/10.1167/tvst.5.2.12>.
30. Garway-Heath DF, Poinoosawmy D, Fitzke FW, Hitchings RA. Mapping the visual field to the optic disc in normal tension glaucoma eyes. *Ophthalmology.* 2000;107:1809–1815. [https://doi.org/10.1016/s0161-6420\(00\)00284-0](https://doi.org/10.1016/s0161-6420(00)00284-0).
31. Åsman P, Heijl A. Glaucoma hemifield test: automated visual field evaluation. *Arch Ophthalmol.* 1992;110:812–819. <https://doi.org/10.1001/archophth.1992.01080180084033>.
32. Nouri-Mahdavi K, Mock D, Hosseini H, et al. Pointwise rates of visual field progression cluster according to retinal nerve fiber layer bundles. *Invest Ophthalmol Vis Sci.* 2012;53:2390–2394. <https://doi.org/10.1167/iovs.11-9021>.
33. Goldbaum MH, Lee I, Jang G, et al. Progression of patterns (POP): a machine classifier algorithm to identify glaucoma progression in visual fields. *Invest Ophthalmol Vis Sci.* 2012;53:6557–6567. <https://doi.org/10.1167/iovs.11-8363>.
34. Goldbaum MH, Sample PA, Zhang Z, et al. Using unsupervised learning with independent component analysis to identify patterns of glaucomatous visual field defects. *Invest Ophthalmol Vis Sci.* 2005;46:3676–3683. <https://doi.org/10.1167/iovs.04-1167>.
35. Sample PA, Boden C, Zhang Z, et al. Unsupervised machine learning with independent component analysis to identify areas of progression in glaucomatous visual fields. *Invest Ophthalmol Vis Sci.* 2005;46:3684–3692. <https://doi.org/10.1167/iovs.04-1168>.
36. Kingma DP, Welling M. Auto-encoding variational bayes. *arXiv Preprint* 2013;ArXiv:13126114.
37. Goodfellow I, Pouget-Abadie J, Mirza M, et al. Generative adversarial nets. *Adv Neural Inf Process Syst.* 2014;27.
38. Hassan ON, Sahin S, Mohammadzadeh V, et al. Conditional GAN for prediction of glaucoma progression with macular optical coherence tomography. *Paper presented at: International Symposium on Visual Computing.* 2020.
39. Berchuck SI, Mukherjee S, Medeiros FA. Estimating rates of progression and predicting future visual fields in glaucoma using a deep variational autoencoder. *Sci Rep.* 2019;9:18113. <https://doi.org/10.1038/s41598-019-54653-6>.
40. Asaoka R, Murata H, Asano S, et al. The usefulness of the deep learning method of variational autoencoder to reduce measurement noise in glaucomatous visual fields. *Sci Rep.* 2020;10:7893. <https://doi.org/10.1038/s41598-020-64869-6>.
41. Asaoka R, Murata H, Matsuura M, Fujino Y, Yanagisawa M, Yamashita T. Improving the structure–function relationship in glaucomatous visual fields by using a deep learning–based noise reduction approach. *Ophthalmol Glaucoma.* 2020;3:210–217. <https://doi.org/10.1016/j.ogla.2020.01.001>.
42. Way GP, Greene CS. Extracting a biologically relevant latent space from cancer transcriptomes with variational autoencoders. *Pacific Symp Biocomput.* 2018;23:80–91.
43. Choi H, Kang H, Lee DS; Alzheimer’s Disease Neuroimaging Initiative. Predicting aging of brain metabolic topography using variational autoencoder. *Front Aging Neurosci.* 2018;10:212. <https://doi.org/10.3389/fnagi.2018.00212>.
44. Marin-Franch I, Swanson WH. The visualFields package: a tool for analysis and visualization of visual fields. *J Vis.* 2013;13:10. <https://doi.org/10.1167/13.4.10>.
45. Kullback S, Leibler RA. On information and sufficiency. *Ann Math Statist.* 1951;22:79–86. <https://doi.org/10.1214/aoms/1177729694>.
46. Kingma DP, Adam BJ. A method for stochastic optimization. *arXiv Preprint.* 2014;ArXiv:14126980.
47. Abadi M, Barham P, Chen J, et al. TensorFlow: a system for large-scale machine learning. Paper presented at: 12th USENIX symposium on operating systems design and implementation; 2016.
48. Rossum GV, Drake FL. *Python 3 Reference Manual.* Scotts Valley, CA: CreateSpace; 2009.
49. Abadi M, Agarwal A, Barham P, et al. Tensorflow: large-scale machine learning on heterogeneous distributed systems. *arXiv Preprint.* 2016;ArXiv:160304467.
50. Virtanen P, Gommers R, Oliphant TE, et al. SciPy 1.0: fundamental algorithms for scientific computing in Python. *Nat Methods.* 2020;17:261–272. <https://doi.org/10.1038/s41592-019-0686-2>.
51. Zaykin DV, Zhivotovsky LA, Westfall PH, Weir BS. Truncated product method for combining P-values. *Genetic Epidemiology: The Official Publication of the International Genetic Epidemiology Society.* *Genet Epidemiol.* 2002;22:170–185. <https://doi.org/10.1002/gepi.0042>.
52. Spry PG, Bates AB, Johnson CA, Chauhan BC. Simulation of longitudinal threshold visual field data. *Invest Ophthalmol Vis Sci.* 2000;41:2192–2200.
53. Gardiner SK, Crabb DP. Examination of different pointwise linear regression methods for determining visual field progression. *Invest Ophthalmol Vis Sci.* 2002;43:1400–1407.
54. Heijl A, Lindgren G, Olsson J. Normal variability of static perimetric threshold values across the central visual field. *Arch*

- Ophthalmol.* 1987;105:1544–1549. <https://doi.org/10.1001/archophth.1987.01060110090039>.
55. Sample PA. Using unsupervised learning with variational bayesian mixture of factor analysis to identify patterns of glaucomatous visual field defects. *Iovs.* 2004;45:2596–2605.
56. Wetzel SJ. Unsupervised learning of phase transitions: from principal component analysis to variational autoencoders. *Phys Rev E.* 2017;96:022140. <https://doi.org/10.1103/PhysRevE.96.022140>.
57. Li Z, He Y, Keel S, Meng W, Chang RT, He M. Efficacy of a deep learning system for detecting glaucomatous optic neuropathy based on color fundus photographs. *Ophthalmology.* 2018;125:1199–1206. <https://doi.org/10.1016/j.ophtha.2018.01.023>.
58. Yousefi S, Kiwaki T, Zheng Y, et al. Detection of longitudinal visual field progression in glaucoma using machine learning. *Am J Ophthalmol.* 2018;193:71–79. <https://doi.org/10.1016/j.ajo.2018.06.007>.
59. Dixit A, Yohannan J, Boland MV. Assessing glaucoma progression using machine learning trained on longitudinal visual field and clinical data. *Ophthalmology.* 2021;128:1016–1026. <https://doi.org/10.1016/j.ophtha.2020.12.020>.
60. Mandava S, Zulauf M, Zeyen T, Caprioli J. An evaluation of clusters in the glaucomatous visual field. *Am J Ophthalmol.* 1993;116:684–691. [https://doi.org/10.1016/s0002-9394\(14\)73466-x](https://doi.org/10.1016/s0002-9394(14)73466-x).
61. De Moraes CG, Liebmann JM, Levin LA. Detection and measurement of clinically meaningful visual field progression in clinical trials for glaucoma. *Prog Retin Eye Res.* 2017;56:107–147. <https://doi.org/10.1016/j.preteyeres.2016.10.001>.
62. Spry PGD, Johnson CA. Identification of progressive glaucomatous visual field loss. *Surv Ophthalmol.* 2002;47:158–173. [https://doi.org/10.1016/s0039-6257\(01\)00299-5](https://doi.org/10.1016/s0039-6257(01)00299-5).
63. Nouri-Mahdavi K, Zarei R, Caprioli J. Influence of visual field testing frequency on detection of glaucoma progression with trend analyses. *Arch Ophthalmol.* 2011;129:1521–1527. <https://doi.org/10.1001/archophthalmol.2011.224>.